Chinese Chemical Letters 33 (2022) 2832–2844

Contents lists available at ScienceDirect

Chinese Chemical Letters

journal homepage: www.elsevier.com/locate/cclet

Recent progress on the smart membranes based on two-dimensional materials

Xinyu Ai[1], Yu-Hao Li[1], Yi-Wei Li[1], Tiantian Gao*, Kai-Ge Zhou*

Institute of Molecular Plus, Tianjin University, Tianjin 300110, China

ARTICLE INFO

Article history:
Received 31 August 2021
Revised 27 September 2021
Accepted 8 October 2021
Available online 14 October 2021

Keywords:
Smart membranes
Two-dimensional material
Tunable nanofluidics
Membrane separation
Blue energy harvesting
Sensor

ABSTRACT

Inspired by the biosystems, the artificial smart membrane to control the mass transport and molecular conversion has attracted increasing attention in the fields of membrane separation, desalination, nanofiltration, healthcare and environmental remediation. However, the trade-off limitations in polymeric membranes greatly hinder the development of smart membranes with high permeability and manipulability. Recently, inspired by the unique physical/chemical properties of two-dimensional (2D) materials, 2D materials-based smart membranes (2DSMs) with the ability of intelligent regulation under different stimuli are highly suitable for membrane applications. According to the desired properties, the 2DSMs with abundant functional groups can be designed through chemical modification to change the original properties and obtain tunable interlayer spacings under different external conditions. In this review, we summarize the recent progress on artificial smart membranes based on 2D materials. The design concept and fabrication strategy of 2DSMs are first introduced. Following that, the developed 2DSMs are introduced and classified by the type of responsive stimuli, including pH, magnetic field, electric field, light and temperature. Then, the 2DSMs exhibiting unique performances as membrane separation, pressure sensors, blue energy harvesting, photoelectrochemical sensors and biomimetic devices are presented. Finally, the perspectives and challenges in the developments of 2DSMs are discussed

1. Introduction

Up to now, various functional membranes to control the mass transport in the natural systems have been discovered, *e.g.*, a group of proteins called aquaporins to manipulate the water transport across the liposome membrane [1], the sodium-potassium pump (Na^+/K^+-ATPase), a series of enzymes pumping sodium and potassium inside or outside cells driven by the hydrolysis of Adenosine triphosphate (ATP) which plays an important role in the mass-to-energy conversion [2]. Inspired by the above natural systems, artificial smart membranes have been designed for applications in membrane separation, healthcare, energy conversion, environmental engineering, *etc.* [3]. An ideal smart membrane should exhibit defined selectivity of molecular transport, high permeability, fast and significant response to the external stimuli and long-term stability [4]. The previous attempts mostly focused on the smart membranes based on responsive polymers, which can adjust the volume or surface charging by pH, temperature, light, electric field electrochemical potential or signal molecules [5,6]. However, most polymeric membranes suffer from the trade-off limitations between permeability and manipulability. In addition, it is a challenge to conquer the swelling of polymeric membranes and plasticizing aging during the operation process [6]. Therefore, to break the above limitations, developing smart membranes based on new concepts and materials is highly desired.

Recently, with the rapid developments in the field of 2D materials [7–9], numerous anomalous nanofluidic phenomena have been discovered in the families of 2D materials, inspiring the design of smart membranes [10,11]. The first unique property of mass transport is the ultrafast transport through the 2D capillary constructed by the assembly of 2D nanosheets. In 2012, Nair *et al.* discovered the resistance-free water permeation through the graphene-oxide lamellar membranes [12]. Then, Radha *et al.* reported that the ballistic transport of gas molecules through the 2D capillary occurs when the De Broglie wavelength of gas molecules is less than the roughness of the 2D materials [13]. The second important property of mass transport in 2D membranes is the size-exclusion selectivity owing to the interlayer space with a typical size between 0.3–2 nm [14–16], defined by the van der Waals, electrostatic or hydrogen-bonding interaction between the layers [12,17]. Thirdly,

* Corresponding authors.
E-mail addresses: gaott@tju.edu.cn (T. Gao), kaigezhou@tju.edu.cn (K.-G. Zhou).
[1] These authors contributed equally to this work.

https://doi.org/10.1016/j.cclet.2021.10.013
1001-8417/

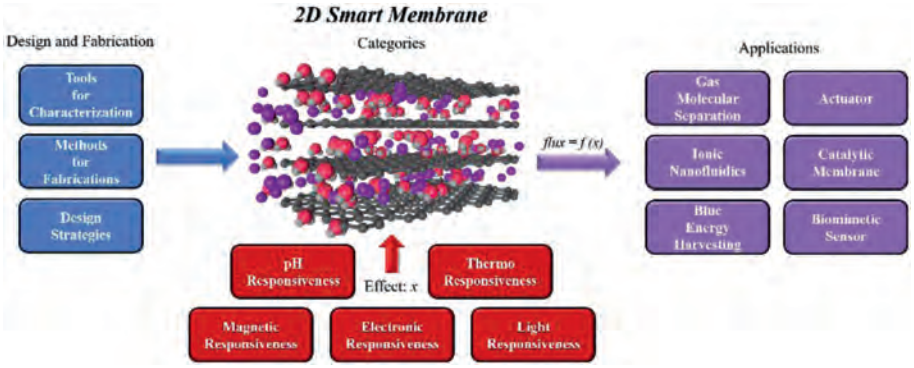

Fig. 1. The scope of this review.

attributed to the sub-nanometer molecular channels confined inside the 2D capillary, the mass transport can be easily tuned by the interface physical or chemical properties [18]. In addition, the expanding families of 2D materials (*e.g.*, graphene oxide (GO) [19], MXene [20–24], hexagonal boron nitride (h-BN) [25], transition metal dichalcogenides (TMDs) [26,27], layered double hydroxides (LDHs) [28], black phosphorus [29]) and non-porous materials (2D zeolites, 2D covalent organic frameworks (COFs) [30,31], 2D metal-organic frameworks (MOFs) [32], graphitic carbon nitride (g-C_3N_4) [33], *etc.*) provides more potential candidates to build up smart membranes.

Taking the above advantages in ultrafast transport, size-dependent selectivity and versatile interfacial properties, 2D materials have attracted increasing attention in the design of smart membranes for membrane separation, desalination, ultrafiltration and healthcare applications.

In this review, we summarize the recent progress in smart membranes based on 2D materials (Fig. 1). The designing strategy and preparation approaches will be firstly introduced. Secondly, the smart membrane based on 2D materials will be classified depending on the responsive stimuli, including pH, magnetic field, electric field, light and temperature. Then, the applications of the 2D smart membrane in the field of membrane separation, pressure sensors, blue energy harvesting, photoelectrochemical sensors and biomimetic devices will be presented.

2. Design and fabrication of 2DSMs

2.1. Design strategies for 2DSMs

So far, there are two main strategies to realize the response of 2DSMs (Fig. 2). One is to tune the interspace size of membranes. When there is an external environmental stimulus, the size change of the intermembrane channel will directly affect the transport of ions, so as to achieve the response to the stimulus. The other is that by tuning the interfacial charging of the membranes. In this way, the surface potential of the membranes can be changed, and then affect ion penetration, achieving the response.

For majorities of the 2DSMs, the response mechanisms have resulted from the tunable surface-charge and channel among the interlayers of 2D nanosheets. Besides the above two strategies, the channel-changing on the 2D plane triggered by the external stimulus can also induce the smart response of the 2DSMs. Zhao *et al.* reported the reversible thermo-triggered molecular sieving membranes composed of 2D metal-organic nanosheets (MAMS-1) for gas separation [34]. The aperture of the pathway that was perpendicular to the 2D basal plane and gated by two pairs of *tert*–butyl groups on the 2D nanosheets demonstrated the reversed thermo-switchable feature due to the dynamic rotation of the *tert*–butyl groups and induced the tunable gas permeation flux and selectivity. Smolyanitsky's team demonstrated the tensile strain-induced response of graphene-based ion channels and nanoporous monolayer MoS_2 membranes through molecular dynamics simulations [35,36]. Both graphene and MoS_2 membranes exhibited high mechanosensitivity and the tensile strain resulted in an even exponential increase of the permeation. The strategy of the channel-changing induced response in 2DSMs and applications still needs further investigation in future.

2.2. Methods for fabrications

Up to now, there have been a variety of 2DSMs preparation methods which can be generally divided into top-down and bottom-up ways. The top-down method refers to exfoliating 2D layers from the bulk materials, while the bottom-up method means the direct synthesis of 2D materials from the basic unit. The top-down method contains intercalation exfoliation and mechanical exfoliation. Intercalation exfoliation is achieved by the entry of ions or molecules into layers to weaken the interlayer interactions or increase the surface charge and eventually promote dispersion in solvents. As a representative, Li^+ ions are used to intercalate into MoS_2 bulk through strong hydration to obtain MoS_2 nanosheets [37]. Mechanical exfoliation relies on mechanical force such as widely used ultrasonication and shear force, showing advantages in good operability, less susceptibility to the environment and precise fabrication [38]. On this basis, Radha's group formed precise, highly controlled single-atom defects on WS_2 films using a 30 kV gallium–sourced focused ion beam (FIB) etching [39]. Taking advantage of the electrochemical activity of molybdenum disulfide, Feng's group developed a convenient and scalable method for the preparation of nanopores by electrochemical reaction (ECR) with sub-nanometer precision, which can continuously remove individual atoms or unit cells from a MoS_2 flake [40]. The bottom-up method mainly includes vacuum filtration, interfacial assembly; In addition, different stacking modes of some 2D materials have an impact on their performance. For instance, different stacking modes of MOF have a significant impact on their gas separation performance. Liu's group formed an ultrathin tetrakis(4-carboxyphenyl)porphyrin (TCPP) derived 2D MOF film with good growth and high c-orientation by the *in-situ* solvothermal method under controlled conditions [40]. The regularly vertical stacking of single Cu-TCPP layers resulted in narrowed pore size and interlocked interlayer gallery, providing the Cu-TCPP film with superb gas selectivity. Thus, the microstructure optimization at the mesoscopic scale in the preparation of 2D membranes is crucial to the ability of precise size-selective molecular sieves.

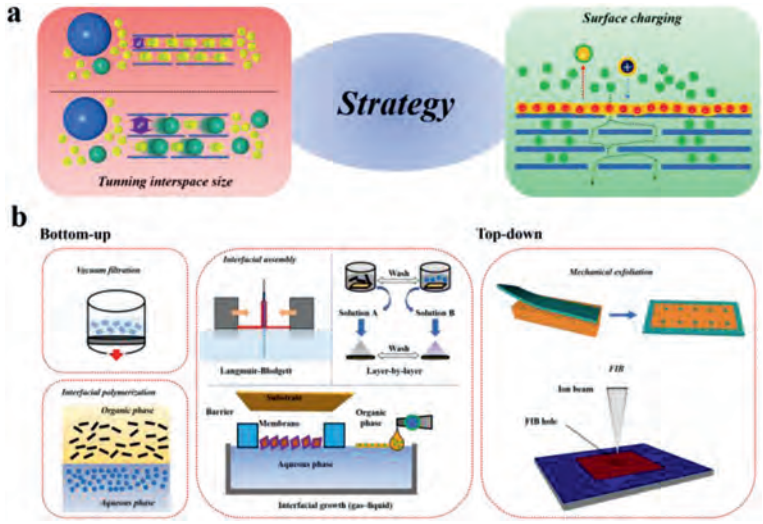

Fig. 2. (a) The strategy of designing 2DSMs. (b) The methods of fabricating 2DSMs.

2.3. Tools for characterization

2D materials have attracted much attentions for a variety of amazing properties. But on the other hand, some traditional characterization methods cannot be used for 2D materials. Limited by the atomically thin nanosheets, the characteristics and functionalities of 2D materials depend strongly on surface chemistry and interfacial coupling effects [41]. Hence, the exploration of advanced characterizations and precise control of surfaces and interfaces are vital to exploit the potentials of 2D materials. Under certain conditions, the surfaces and interfaces of the atomical thin layers are optically and electronically transparent, which can be characterized through the spectrum and microscopy-related techniques.

Scanning tunneling microscopy (STM) is one of the most significant tools for characterizing surfaces of 2D materials. For example, electrons generated by STM can enter through monolayer h-BN into underlying conductors [42]. STM topography images show the convolution of structure and electronic properties, which complicate the identification of the atomic arrangements in space. Although the STM images are usually far less detailed than the actual atomic structure, the STM tips can be functionalized by other methods and probes such as carbon monoxide (CO) in order to improve spatial resolution [43]. In the standard STM imaging model, the heterostructures between pristine and fluorenone-functionalized graphene nanoribbons (GNRs) are indistinguishable. In comparison, the STM with tips functionalized by CO can be used to easily identify these heterostructures [44]. Unlike STM based on the volage between tips and surfaces, atomic force microscopy (AFM) functions by the van der Waals interactions between tips and sample surfaces. Along the horizontal direction, two adjacent layers may be difficult to distinguish due to the atomically thin thickness, while the height differences of the edges can be used to identify the interfaces between adjacent nanosheets. Monolayer and bilayer graphene region fabricated by epitaxial growth on SiC can be distinguished by phase mapping [45]. On the large scale, lateral force microscopy (LFM) can distinguish different materials or friction anisotropies. The image of the same monolayer graphene exfoliated on SiO_2 showed domain structure [46]. Similar to STM, the AFM tip with an external voltage applied can produce local electronic coupling to the sample. Such as electrostatic force microscopy (EFM) [47,48] and Kelvin probe force microscopy (KPFM) [49–54], the electronic coupling can adjust force measurements and may directly output image signal in conductive AFM (C-AFM) [55–59]. With the development of advanced characterization, the research on 2D materials has gained better understanding and promote their practical potentials.

In addition, molecular dynamics simulations can predict or explain 2D material transport characteristics. David *et al.* used classical molecular dynamics simulation to explore how single-layer or multilayer nanoporous graphene (NPG) can be used as a reverse osmosis membrane in seawater desalination, and tested the response of the membrane to these changes by changing the layer spacing, pore position and external force applied to the system [60]. After each simulation, they calculated the flow rate by counting the number of water molecules and salt ions in the feed, interlayer space and infiltration zones in a period of time which was set as reference. The water flows rate increased with the pressure, and it can be seen that the membrane showed a positive response to the pressure change. When the layer spacing was less than 8 Å, the layer spacing and the water flow rate decreased, indicating that the film had a positive response to the change of layer spacing. Nieszporek *et al.* studied the permeability of graphene sheets with designed nanopore using classical molecular dynamics [61]. They used two graphene sheets of the same box size, located at $z = 4$ nm and $z = 12$ nm, and applied a constant volume analog box. The gas mixture consisting of alkane molecules was placed below and above the graphene (retention area), with a permeation area in the 4–12 nm range (initial vacuum). They investigated the effect of temperature on the simulation results. When the temperature rised, the methane permeation rate increased obviously, indicating a positive response to the temperature changes.

3. Categories of smart responsive 2D membranes

3.1. pH responsive membranes

Based on previous research, pH-responsive materials have a wide range of applications, such as separating water from oil [62], changing the hydrophilicity of surfaces [63], mechanical strength adjustment [64]. Most of the pH-responsive materials are long-chain organic macromolecules. Inspired by these materials, the researchers combined them with 2D materials such as GO to design pH-responsive membranes. The pH-responsive membranes work in two ways. One way is through changing the electrical properties or charges on the surface or inside of the membrane under pH stimulus. Thus, the ion permeability of the membrane can be tuned by changing its surface charging properties. The other way refers to the change of molecular structures by pH, which can induce the

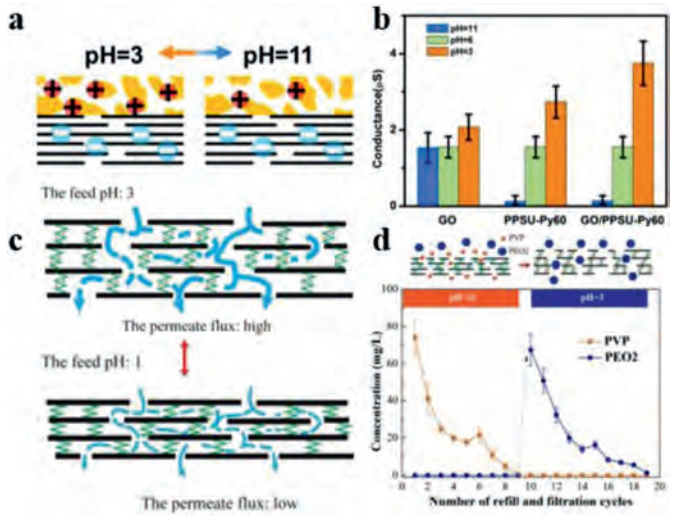

Fig. 3. (a) Schematic depiction of the surface charge density of the heterogeneous membrane in different pH environments. (b) Histogram of the ionic conductance in different pH environment calculated from the *I*–*V* curves. (a, b) Reprinted with permission [65]. Copyright 2017, American Chemical Society. (c) Schematic of the structure change in the GO/PEI pH-responsive membrane at pH 3 and 11. (d) The concentration of PVP and PEO2 in the permeate solution at pH 11 and 3 during the filtration process (the schematic diagram of the separation process was shown above). (c, d) Reprinted with permission [66]. Copyright 2019, American Chemical Society.

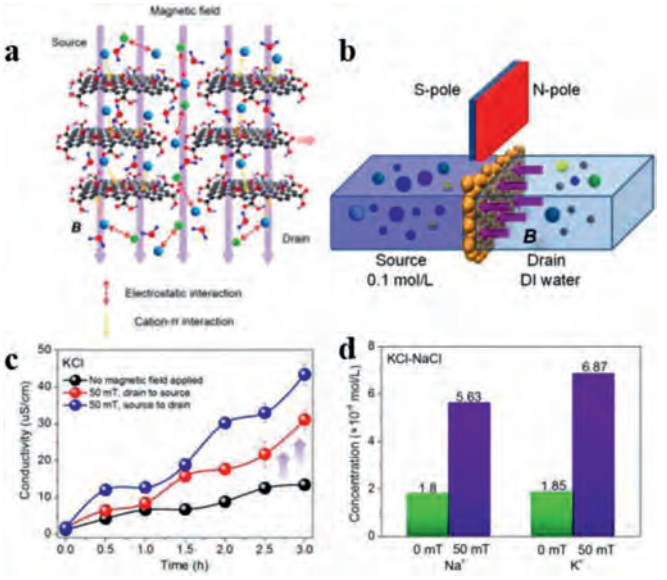

Fig. 4. (a) Schematic diagram of ion transport through GO membranes under the applied magnetic field. (b) The mechanism proposed for the magneto-induced transmembrane transport of ions through GO membranes. (c) The conductivity variations of the KCl drains after applying external magnetic fields with different directions. (d) Ion concentrations of the drains during the permeation test of KCl and NaCl with and without the external magnetic field. Reprinted with permission [73]. Copyright 2014, Springer Nature Publishing Group.

varied interlayer spacings of the 2D membrane and tunable permeance of molecules or ions.

In 2017, Lei Jiang's group developed a polymer/GO heterogeneous membrane with adjustable charge density by varying pH [65]. As shown in Figs. 3a and b, the heterogeneous membrane can increase the positively charged density on the membrane surface with the decrease of pH around the membrane, which can significantly affect the permeability of the membrane. This work is an earlier work focused on pH-responsive membrane with regulated permeability and good separation effect by changing electrical properties.

In addition to regulating the membrane permeability by changing electrical properties by pH, the pH-responsive membrane based on the changeable molecular structures by pH has also been reported in recent years. Chen *et al.* developed the stable GO/polyetherimide (GO/PEI) membrane with pH-responsiveness for advanced molecular separation applications [66,67]. As shown in Figs. 3c and d, the membrane was made of GO, which was crosslinked by PEI molecules with significant responsiveness to pH. With the increase of pH, PEI molecular could shrink, which leads to the reduction of the interlayer spacing. Thus, the permeability of the membrane was changed and molecular with different sizes can permeate through the membrane at different pH. This work makes it possible to screen molecules of different sizes.

Recently, a novel membrane composed of GO and polyamine macromolecules (PA) was reported to have reverse responsiveness to pH compared with the above reports [67]. The membrane has a similar structure to the above membrane. Unlike other typical membranes, the permeability of the GO/PA composite membrane was only determined by the protonation states of the membrane structure and specific interactions with other ions rather than pore size and external pressure. In addition, the permeability of some ions can be tuned by the existence of other certain ions, providing the composite membrane with a transistor effect for selective ion transport.

Besides the pH induced responsiveness, charged ions have been reported to tune the nanochannels of the GO membrane. Fang *et al.* reported precise cationic control of the interlayer spacing of GO membrane with Å precision using K^+, Na^+, Ca^{2+}, Li^+ and Mg^{2+} ions [68]. The GO membrane controlled by one kind of cation exhibited efficient exclusion of other cations with larger hydrated volumes. The tunable interlayer spacing by cations resulted from the strong cation-π interactions with GO sheets.

In brief, the environmental conditions can be easily regulated by changing the pH conditions which is of high adjustment accuracy, making it a promising strategy for smart 2D membranes.

3.2. Magnetic responsive membranes

As a remote controlling method, magnetic field can be also applied to manipulate the permeation and selectivity of membranes. For instance, Yang *et al.* grafted the Fe_3O_4 nanoparticles into the polymer matrix in order to enhance the permeation and salt rejection [69]. The polymer chain attached on superparamagnetic nanoparticles was driven and folded by the oscillating magnetic field as a valve. Recent studies also indicate that graphene related 2D materials could exhibits ferromagnetism or weak antiferromagnetism at room temperature [70–72]. As a result, the orientation of the 2D nanosheets can be potentially tuned by the external magnetic field, and then affect the geometry and packing order of the 2D nanocapillaries.

In 2004, Sun *et al.* for the first time reported a magnetic responsive membrane constructed by the ferromagnetic graphene oxide lamellar (Figs. 4a and b) [73]. Apart from the proton, the cation penetration rate across the GO lamellar was polar-independently enhanced by 3–4 times under external magnetostatic field (Figs. 4c and d). They attributed the enhancement to the better packing order between the GO layers in the lamellar and the shorter transport pathway under magnetostatic field. Therefore, the transport of cations in the "vehicle" way becomes easier along the well-packed 2D nanocapillary driven by the magnetostatic field. In contrast, the protons rapidly mobilize along the water chain inside the lamellar in Grotthuss mechanism. Consequently, the permeation rate of proton is determined by the exchanging barrier between the neigh-

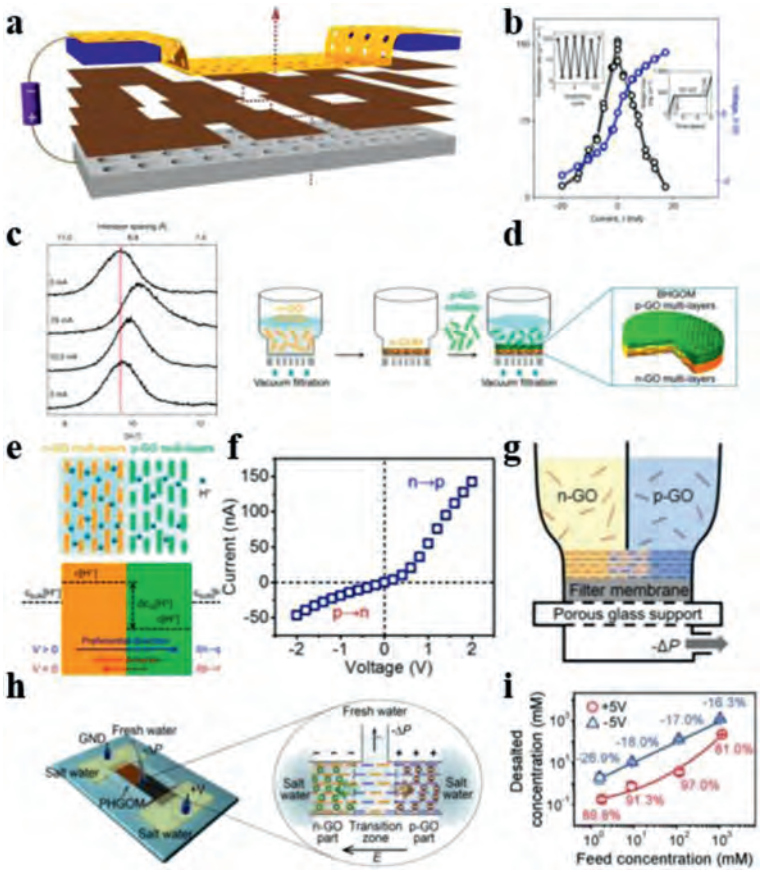

Fig. 5. (a) Schematic illustration of the GO membrane on a porous silver substrate under the external applied voltage. (b) Water permeation rate as a function of the current of the GO membrane after the filament formation and the corresponding *I–V* characteristics (color-coded axes). (c) The XRD patterns and interlayer spacings of the GO membrane under different currents. (a-c) Reprinted with permission [79]. Copyright 2018, Springer Nature Publishing Group. (d) Schematic demonstration of the sequential filtration process for the fabrication of BHGOM. (e) Scheme of the mechanism for asymmetric proton transport through BHGOM driven by electric field. (f) The current−voltage curve of BHGOM with rectified proton transport at 1 mmol/L HCl solution. (d-f) Reprinted with permission [82]. Copyright 2019, American Chemical Society. (g) Scheme of the dual-flow filtration setup for fabrication of the PHGOM. (h) Scheme of the working mechanism for deionized water extraction from the PHGOM. (i) The desalted concentration in extracted water and corresponding salt rejection rates (R) of the PHGOM under forward and reverse bias of 5 V at various feed concentrations of NaCl solution. (g-i) Reprinted with permission [83]. Copyright 2020, Wiley-VCH.

boring water molecules, and rarely affected by the magnetostatic field. Similar magnetostatic enhancement has also been found in GO/Fe_3O_4 forward osmosis membranes [74]. Although the response of mass transport to the magnetic field are comparably weak, the remote control and low energy consumption still makes the magnetic responsive membranes attractive. Therefore, new designing strategies or magnetic 2D materials (*e.g.*, CrI_3, Fe_3GeTe_2 and $FePS_3$) may be introduced [75].

3.3. Electronic responsive membranes

The electric responsive membranes are controlled by electrical energy which is the most widely used energy, thereby having attracted extensive attention recently. The most common material for electric responsive membranes is GO. Because of its good stability and mechanical strength, the electric responsive membrane made of GO can be used in the fields of gas separation [76], ion separation [77,78] and so on. On the basis of its working principle, the electric responsive membrane can be roughly divided into two categories: one kind is to change the size of the 2D channels, the other is to change the charge distribution.

In 2018, Zhou *et al*. developed an electrically responsive GO membrane [79]. As shown in Figs. 5a-c, in this work, various characterization methods were applied to rigorously prove the electric responsiveness of GO films, and very considerable controllability was obtained. This work reported the precise control of water permeation simply by introducing the external voltage or electric field, paving the way for the development of smart membrane technologies for filtration and artificial biological systems.

Since then, the research of GO in electrically responsive smart membranes has become increasingly popular. Li *et al*. reported the collective electrolyte gating effect of multilayer reduced graphene oxide membranes (MGM) in the conventional symmetric supercapacitor [80]. The curve of G_{MGM}-V_g exhibited a non-monotonic relationship, indicating the back-gated field effect. The minimum G_{MGM} during the positive polarization ($V_g > 0$) could be attributed to the shift of the Dirac point of rGO and the electrostatic interactions between the rGO sheets and the electrolyte. The electrolyte gating effect revealed the nanoconfinement-dependent hysteresis and the non-linear response of the G_{MGM} to voltage indicated the memory effect, extending potentials of 2D materials for novel devices.

Besides graphene, other 2D materials such as MXene also have been reported as the electrically responsive membrane [81]. The ion transport was in the transverse direction of the MXene membrane. The ion transport was significantly suppressed under the negative V_g because negative potential made the nanochannels attract more positive counterions and the strong interactions between ions and nanochannels slowed down ion migration. By comparison, the positive V_g promoted the ion transport through the MXene membrane. The maximum on-off ratio of the membrane can be approximately 10 by applying different external voltages.

Other than the symmetric membrane, the asymmetric membrane with heterojunction structure was composed of two different materials and has shown unique properties as the electrically responsive membrane. Derived from the different properties of the two materials, the transport behavior of ions depended on the migration direction across the asymmetric membrane. From Fig. 5d, Guo's group developed a heterojunction type of graphene-based electrically responsive membrane, which was consisted of sequentially stacked positively charged GO (p-GO) and negatively charged GO (n-GO) layers [82]. On the basis of electrostatic interactions between GO and protons, the n-GO part with the negatively charged surface can attract more protons, showing higher proton concentration than that of the p-GO part in the bilayered heterogeneous GO membrane (BHGOM). The difference in concentration led to the internal proton concentration gradient ($\Delta c_{in}[H^+]$) and internal electric field, which determined the preferential direction of proton transport from n-GO to p-GO part (Figs. 5e and f). Further, Guo's group reported a novel planar heterogeneous graphene oxide membrane (PHGOM) [83]. In the lateral direction, the PHGOM was composed of distinct n-GO parts and p-GO parts, which were separated by the transition zone (Fig. 5g). As shown in Fig. 5h, the asymmetric structure formed an internal electric field with the direction from p-GO to n-GO. Accompanied with the electrostatic attraction, positively charged ions gathered in the nanochannels formed by n-GO nanosheets and anions were attracted by p-GO nanosheets. Thus, both cations and anions were restricted in the nanochannels of the asymmetric membrane under the electric field force and electrostatic interaction. Impressively, the rejection for NaCl of the heterogeneous membrane reached 97% under a forward bias of 5 V (Fig. 5i). By contrast, the salt concentration of the transition zone was higher than that of the feed solution under a reverse bias, showing negative rejections and the concentration effect.

There are many advantages of using electricity or voltage as the stimulus in the responsive membrane, such as easily adjustable and convenient. Thus, the development of electrically responsive membrane is vital to 2D materials. In addition, it is of great significance to engineer the fine structure and composition of the interfaces for the electrically responsive membrane to extend its practical applications such as desalination and ion rectification devices.

3.4. Light responsive membranes

In recent years, light-responsive membranes have attracted extensive attention owing to the environmental friendness and easy accessibility of light energy such as being environmentally friendly and easily accessible. Materials commonly used to make photoresponsive films include C_3N_4 [84], GO [85], MXene [86], *etc.* The light-responsive membrane can be divided into two categories based on its working principle: one is to change the potential state in the membrane, and the other is to change the internal structure of the membrane.

Based on the intrinsic photothermal properties of MXene, Luo demonstrated the MXene membrane with tunable ionic conductivity by laser light [86]. The MXene membrane exhibited good stability in water with a certain extent of water molecules existing in the 2D nanochannels of the membrane. In the absence of laser light, ions can transport water freely in the lateral direction of 2D nanochannels (Fig. 6a). When the laser light was applied, the MXene membrane converted the laser light to heat resulted in evaporation of water molecules within the nanochannel of the irradiated part, thereby completely cutting off the migration of water and ions (Fig. 6b). In addition, the MXene membrane showed reversible and repeatable responsiveness to the laser light and could still continue to migrate ions after removal of the laser (Fig. 6c). The light-controlled ion transport of the MXene membrane with good stability raises the possibility of designing 2D nanofluidic membranes and extends further applications.

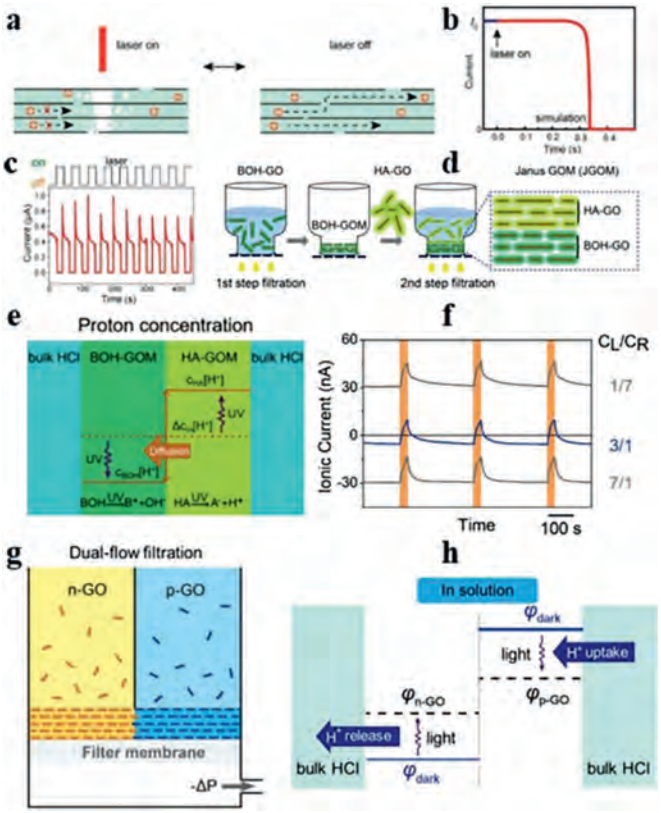

Fig. 6. (a) Schematic of the photo-controlled transport mechanism in the MXene membrane. (b) The rapid response of ionic current from its initial value (I_0) to zero under the laser stimulus. (c) Rapid and reversible switch of the ion transport. (a-c) Reprinted with permission [86]. Copyright 2018, American Chemical Society. (d) A scheme of the two-step filtration process for fabrication of JGOM (Janus GOM). (e) Scheme of proton concentration profile upon UV illumination. (f) Time traces of the ionic current generated by the JGOM at preset concentration gradient. (d-f) Reprinted with permission [87]. Copyright 2019, Wiley-VCH. (g) Scheme of the dual-flow filtration process for fabricating the planar heterogeneous membrane. (h) Schematic diagram of the electric potential of n-GO and p-GO parts in solution before and after the light illumination. (g, h) Reprinted with permission [89]. Copyright, 2020 Wiley-VCH.

On the basis of heterogeneous structure, Guo's group reported the light-responsive graphene oxide Janus membrane composed of photo-sensitive molecules modified GO (BOH-GO) and photoacid molecules modified GO (HA-GO) (Fig. 6d) [87]. In the absence of light, proton concentrations in the membrane of BOH-GO and HA-GO parts were almost identical because of the nearly equal surface charge properties (Fig. 6e). Upon the ultraviolet light, BOH-GOM and HA-GOM exhibited different photoisomerization reactions, inducing the release of OH^- in the BOH-GOM and H^+ in the HA-GOM. The different products under ultraviolet light of the BOH-GO and HA-GO established a proton concentration gradient inside the membrane, which promoted the diffusion of the proton through the membrane. With appropriate concentration, the proton current can even change its direction under ultraviolet light, demonstrating the anti-gradient transport of proton (Fig. 6f).

In 2020, Jiang's group reported a photosensitive homogeneous membrane composed of graphene oxide quantum dots (GOQDs) and reduced graphene oxide (rGO) [88]. Upon the asymmetric light illumination, the photocurrent through the membrane flew from the illuminated part to the non-illuminated part. When the left half of the membrane was illuminated, photo-excited electrons and holes were generated and separated in this left part. Thus, the

concentrations of electrons and holes in the right half were much lower than those in the left, resulting in the carrier transport from the left to the right. The difference in the mobility and diffusivity of photo-excited electrons and holes resulted in the asymmetric carrier transport and unequal electric potentials in the illuminated and non-illuminated parts. In addition, the proportion of GOQDs in the composite membrane also had a great effect on the photocurrent. The addition of GOQDs reduced the interlayer distance of the defect domain between the rGO layers and improved the net ion flux under ultraviolet light. Based on the light-controlled characteristic, the ion transport can be even against the concentration gradient.

Among above reports, the light-responsiveness is formed by setting the asymmetric illuminated and non-illuminated regions. Recently, Guo's group developed a light responsive membrane based on the planar heterogeneous structure reported previously. As shown in Fig. 6g, the composite membrane was composed of positively charged GO (p-GO) and negatively charged GO (n-GO) [89]. In the absence of light, the significant difference of potentials on both sides of the membrane was formed because of different charge types of n-GO and p-GO (Fig. 6h). Upon the light stimulus, the decreased potential provided the p-GO part with less positive charges, resulting in more protons from the bulk solution attracted into the p-GO part.

Besides laser, ultraviolet light and visible light, sunlight can also induce responsiveness. Based on the reliable photothermal properties of graphene, Qu *et al*. reported the solar and thermal responsive membrane composed of microstructured graphene and poly(*N*-isopropyl acrylamide) (mG/PNIPAM) in intelligent solar water evaporation [90]. As the solar intensity varied, the microstructure of the composite membrane achieved reversible transformations resembling the stomal opening and closing of leaves. This composite membrane provides an intelligent material platform with self-adaptability in sunlight-responsive devices.

Other 2D materials including MXene also exhibit excellent photothermal conversion properties. Alshareef's team demonstrated ionic thermoelectric transport through lamellar MXene membranes as the biomimetic thermosensitive nanofluidic platform [91]. Under the local sunlight exposure, the temperature gradient was created within the nanoconfined channels of MXene membranes. The chemical potentials resulted from the temperature gradient induced the thermo-osmotic ion transport and the generation of ionic thermoelectric voltage through the nanoconfined MXene channels. The thermoelectric response sensitivity of MXene membranes was comparable to that of biological thermo-sensation channels.

Solar energy is one of the inexhaustible nature energies. However, most light-responsive membranes reported previously are triggered by laser or ultraviolet light. Because of the global shortage of freshwater, utilizing solar energy maximumly to produce clean water is still a huge challenge. Thus, it is of great importance and meaning to exploit solar triggered responsive membranes and extend practical applications such as nanofluidic devices.

3.5. Thermo responsive membranes

In nature, varieties of plants exhibit self-adaptive functions under various environments. For example, gramineous plans can curl leaves to reduce water loss at noon. The responses of plants to thermal changes are vital to sustaining life. Thus, it is important to develop artificial thermal responsive membranes for biomimetic devices and further applications. Moreover, 2D materials with suitable interlayer spacing and unique 2D nanochannels are conducive to the transport of proton and other substances and have shown potentials in thermal responsive membranes [9]. Pure 2D materials usually exhibit no responsiveness to the thermal stimulus. Nevertheless, by chemical modification or reaction with other thermal responsive molecules or polymers, 2D materials such as GO with abundant oxygen groups can be endowed with corresponding response properties and diverse transport characteristics.

Yang's team reported the positive temperature-responsiveness GO-based membrane with enhanced proton conductivity by intercalating single-strand deoxyribonucleic acid (ssDNA) into the GO layer (Fig. 7a) [92]. As shown in Fig. 7b, the proton conductivity of the DNA@GO-X membrane was enhanced compared with that of the pure GO membrane and the highest proton conductivity was achieved with the amount of DNA solution of 15 mL. More importantly, the proton conductivity with any addition of ssDNA was positively correlated with temperature, which was attributed to the thermal activation characteristics of proton conduction behavior.

In addition, Shen's group introduced another route that intercalated hydrogels between GO layers [93]. Loosely shaped hydrogels could be perfectly embedded between two GO sheets by changing their shape, and could also act as a bond between GO and the substrate. As shown in Fig. 7c, when the temperature increased above the volume phase transition temperature (VPTT), intermolecular hydrogen bonds were formed between NIPAM groups and NIPAM groups, NIPAM groups and methyl acrylic acid (MAA) groups, and MAA groups and MAA groups, resulting in the contraction of the polymer chain and the reduction of microgel volume. Thus, the water flux through the membrane layer increased to 4.5 times of the previous (Fig. 7d), presenting good thermal responsive characteristics. When the temperature decreased lower than the VPTT, the volume of the microgel increased, the channel size decreased and the water flux decreased due to the water expansion of the NIPAM groups and the formation of hydrogen bonds between the amide group and the water molecule.

Because of the excellent photothermal properties of GO, the remote control of membrane permeability was also realized by near-infrared (NIR) light. When P-GOMs were exposed to NIR light, the increased temperature above the lower critical solution temperature (LCST) resulted in the narrowed channel of P-GOMs and reduced water permeability. In 2019, Zhao *et al*. reported the GO-PNIPAM membranes with reversible positive/negative gating regularity by simply tuning the molecule grafting density [94]. By integrating a positive response membrane and a negative response membrane, a bidirectional fluidic controlling membrane system was demonstrated as a self-adaptive gating reactor, paving a way in micro/nanofluidic valves and biochemical reactors.

Other than positive responsiveness to temperature, Liu's team imitated the natural phenomenon of leaves closing stomata at high temperature and prepared the negative temperature-responsive membranes by grafting PNIPAM on the GO sheets [95]. It could be seen from Fig. 7e that PNIPAM chains covalently bound to GO layers formed a hydrogen bond network with water molecules at low temperatures, thus improving water transmittance. When the temperature increased to the LCST [96], adjacent PNIPAM chains would form intramolecular and intermolecular hydrogen bonds, leading to a reduction in channel size and water transmittance [97]. As shown in Fig. 7f, the above two control groups exhibited a positive response to temperature, only the membranes with PNIPAM copolymerized on GO sheets (P-GOMs) exhibited the unique effect of negative response.

Compared with traditional 2D materials such as GO, MOF nanosheet is a new type of metal ions and organic ligands nanomaterials, which has excellent permeability and high selectivity. In addition, MOF nanosheets are easily functionalized by polymers, providing MOF nanosheets with a superior advantage in precisely adjusting the interlayer properties and balanced stability and thermal responsiveness of the membrane. Sun's group reported the first example of thermally reactive and interfacially stable MOF (trZT-MOF; "tr" for thermal reaction) nanosheets [98]. They intro-

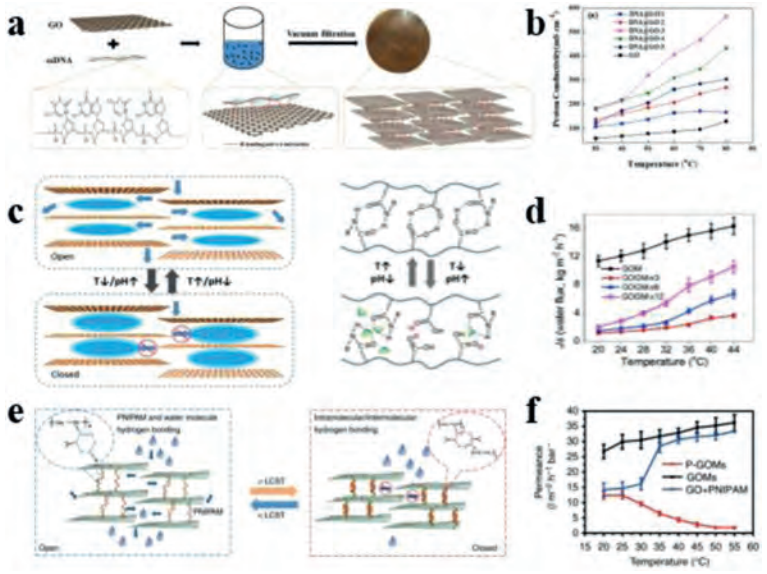

Fig. 7. (a) Schematic illustration of the preparation process of DNA@GO membranes and the digital image of the DNA@GO-3 membrane. (b) Result for the temperature-dependent proton conductivities at 98% RH of the prepared membranes. (a, b) Reprinted with permission [92]. Copyright 2020, Elsevier. (c) Schematic illustration of the mechanism of GO/hydrogel composite membranes (GOGMs). (d) Thermo-responsive gating ratios (RT) of GOGMs with different membrane thicknesses. (c, d) Reprinted with permission [93]. Copyright 2020, Elsevier. (e) Schematic illustration of channel size change of P-GOMs from D1 to D2 caused by the swelling or shrinking of PNIPAM chains covalent bound to GO sheets. (f) Temperature-dependent water permeance curves of GOMs, P-GOMs and physically blending PNIPAM/GO membranes, P-GOMs show the unique negative temperature-responsive coefficient, which is opposite to the positive coefficient of GOMs and GO/PNIPAM blending membrane. Error bars, s.d. ($n = 3$). (e, f) Reprinted with permission [95]. Copyright 2017, Springer Nature Publishing Group.

duced the poly(*N*-vinyl caprolactam) (PVCL) chain in the system. Due to the LCST performance of the PVCL chain, the trZT-MOF has excellent thermal responsive characteristics. The pure water permeance of the trZT-MOF nanosheet membrane is positively responsive to temperature changes, which increases from 858 L m^{-2} h^{-1} bar^{-1} at 20 °C to 1934 L m^{-2} h^{-1} bar^{-1} at 70 °C.

2D materials-based thermal responsive membranes show excellent performance in water and proton transmittance. It is of great value to test different intercalation groups between membranes in order to study the different effects on different substances' transport.

4. Applications

4.1. Gas molecular separation

In industrial procedures, separation of gas mixtures is essential and has played vital roles in the purification of hydrogen (H_2/CO, H_2/CO_2, H_2/N_2, *etc.*) [99–102] and CO_2 capture (CO_2/air, CO_2/H_2) [103–106]. Much attention has been focused on 2D material-based membranes with tunable structures, which are suitable for gas separation. Gas separation is much more defect-sensitive than other separation processes, slight variation of interlayer distance and its chemical environment result in different permeance. Small gas molecular (*e.g.*, He) cannot permeate through GO membranes in the dry state, but high CO_2/N_2 selectivity can be achieved under the high ambient humidity [107]. By taking advantage of the characteristic that the interlayer distance of GO membranes changes with the environment humidity, the stacking structure in the membrane can be accurately adjusted, improving the separation factors and flow rates. Besides GO nanosheets [108–110], many types of 2D nanosheets can be assembled in gas separation membranes, like zeolites [111–113], MXene [114–116], COFs [117–120], *etc.* Most pristine 2D material-based membranes can be modified to achieve different abilities than before, but the change is irreversible. It can synchronously change the performance of gas separation with the various external conditions, which makes it more practical.

In order to break the restricted condition of trade-off, besides achieving the thinner thickness of 2D material-based membranes, using porous 2D nanosheets to avoid the situation that the gas pathways are at least three orders of magnitude higher than the membrane thickness. 2D MOF membranes show great gas separation performance [121,122]. Zhao's group reported a kind of MOF nanosheets named MAMS-1 (Mesh Adjustable Molecular Sieve, $Ni_8(5\text{-bbdc})_6(\mu\text{-OH})_4$), and fabricated MAMS-1 nanosheets into 2D membranes for gas separation [34]. As shown in Fig. 8a, the permeance of MAMS-1 membranes showed negative and switchable responsiveness to temperature between −196 °C to 22 °C, the separation factor varied with temperature, due to the intensified thermal vibration of the *tert*–butyl groups [123] showed in Fig. 8b. At room temperature, *tert*–butyl could rotate freely to change the surrounding free volume (Fig. 8c).

4.2. Ionic nanofluidics

Membranes assembled by 2D materials with regular nanochannel could create micro-/nano-environments to promote molecular and ion separation. The size of the nanochannel in the membrane is about 3–20 Å. In fact, the separation performance of some 2DSMs far exceeds the existing polymer membranes [124,125]. By chemical modification or other methods, nanochannel can be provided with the response to external stimuli to increase the possibility of 2DSMs materials in other applications. A nanofluidic model with optical switch ion current rectification (ICR) by dropping a droplet of spiropyran (SP) solution onto the top surface of the GO membranes (SP-GOM) and SP-GOM showed excellent reversibility in ion transport behavior, which could be switched between high- and low-rectifying states for multiple cycles [126]. This method may provide a new strategy for constructing smart devices based on a 2D nanofluidic model. Besides the light stimulus, smart 2DSMs can also show different ion separation properties under electrical stimulation.

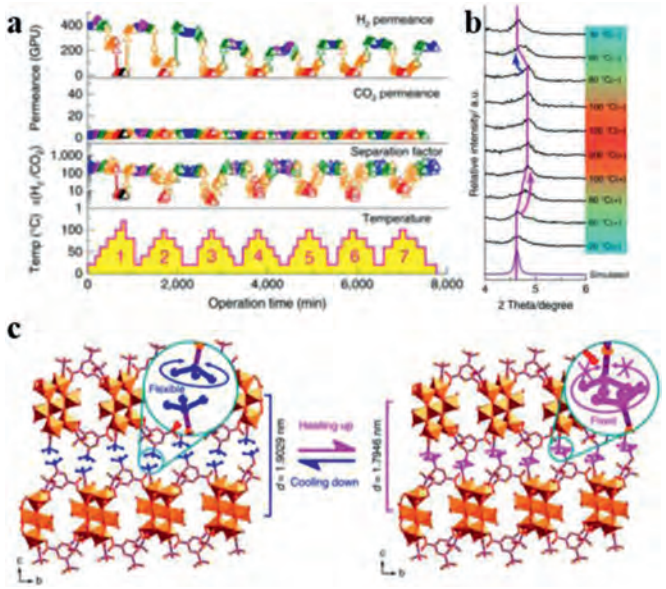

Fig. 8. (a) Gas permeance and H_2/CO_2 separation factors of the 40 nm MAMS-1 membrane under seven heating/cooling cycles. Different colors represent various temperatures: blue, 20 °C; magenta, 40 °C; olive, 60 °C; orange, 80 °C; red, 100 °C and black, 120 °C. (b) Illustration of the expansion (during heating) and shrinkage (during cooling) in ab planes of MAMS-1. The magenta arrows indicate the expansion during heating and the blue arrows indicate the shrinkage during cooling. (c) Illustration of the shrinkage (during heating) and expansion (during cooling) of interlayer distance in MAMS-1. The freely rotated *tert*–butyl groups are highlighted in blue and the frozen ones are highlighted in magenta. Reprinted with permission [123]. Copyright 2017, Springer Nature Publishing Group.

Li's group found that the ionic diffusion flow increased with the rise of the electronic potential of the graphene membrane [127], the new phenomenon was contrary to the classical Poisson-Boltzmann theory and the traditional experimental results. The constrained ions diffusion could be strongly regulated by interfacial electric bilayer (EDL) due to the narrow size of nanochannel in graphene membrane (<2 nm), the test model and reversible modulation were shown in Figs. 9a and b, respectively.

Based on the unique characteristic of 2D membranes in ion migration, 2D materials are excellent platforms for ion conduction and the tunable permeation rates through modification under different stimuli make it possible to extend further practical applications such as rectification devices.

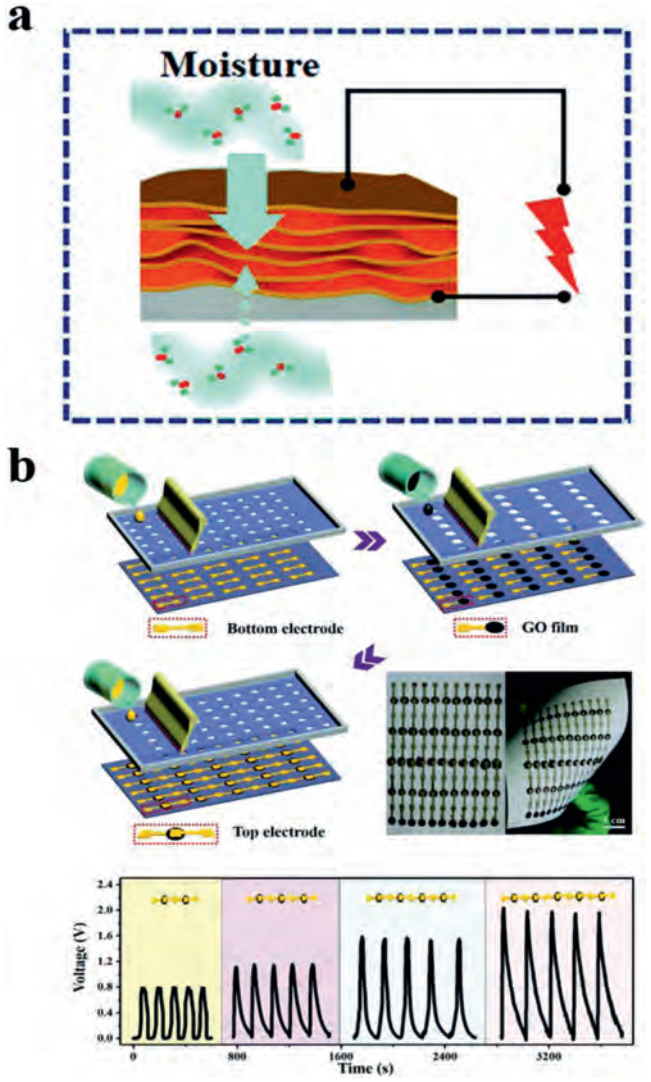

Fig. 9. (a) Schematic diagram of the asymmetric-stimulus-induced potential. (b) Schematic diagram of the procedure for the large-scale fabrication of GO power-generating device arrays on paper and voltage outputs generated by two, three, four and five units connected in series under moisture stimulation of ΔRH = 70% (relative humidity), respectively. Reprinted with permission [129]. Copyright 2018, Royal Society of chemistry.

4.3. Blue energy harvesting

The oceans contain huge amounts of energy, known as "blue energy". In theory, the ocean could meet all of the earth's energy needs without polluting the atmosphere, providing a sustainable and permanent solution to the world's energy needs. Taking advantage of the osmotic pressure difference between fresh water and seawater, Feng's group demonstrated a single-layer MoS_2 nanopore as the osmotic nanogenerator generator [128]. The porous MoS_2 film has better water transport characteristics because of the electrochemical reaction of the MoS_2 nanopores during the preparation process. The osmotic power is generated by separating two reservoirs containing potassium chloride (KCl) solutions of different concentrations with a freestanding MoS_2 membrane, into which a single nanopore has been introduced. Two different concentrations of solution appear chemical potential gradient at the interface of the nanopore and drive the ions to spontaneously pass through the nanopore, forming osmotic ion flux towards the equilibrium state. The presence of surface charges on the pores selects these ions according to the polarity of charge passing through them, resulting in a net measurable osmotic current known as reverse electrodialysis. On this basis, a self-powered nano-system with monolayer porous MoS_2 as a nano-power source was established. Qu's group introduced the self-charging properties of GO films by constructing asymmetric moisturizers on both sides of GO (Fig. 9a), which allowed H^+ to migrate in a directional manner through GO flakes [129]. On this basis, a three-step printing technique was used to create an array of GO power generation devices (Fig. 9b). By properly connecting the power generation devices in series, a steady increase in power output was achieved. Induced voltages of 0.8 V, 1.2 V, 1.6 V and 2.0 V were observed in 2, 3, 4 and 5 series connected-devices respectively.

4.4. Biomimetic sensor

The photoelectrochemical (PEC) sensor is a novel technology that takes light as the excitation source and quantitatively analyzes the relationship between the measured object and the photocurrent or photovoltage by means of electrochemistry and biological recognition. Early PEC sensors generally matched with the

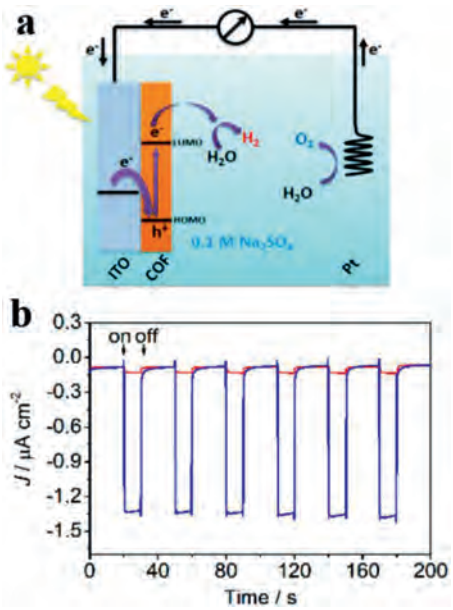

Fig. 10. (a) Schematic for photocurrent generation process of $COF_{TTA\text{-}DHTA}$ film on ITO electrode. (b) Photocurrent responses of blank ITO (red curve) and $COF_{TTA\text{-}DHTA}$ film electrode (blue curve), in the presence of 0.5 mmol/L ascorbic acid with on−off illumination under Xe lamp irradiation. Reprinted with permission [138]. Copyright 2018, American Chemical Society.

disadvantages of poor specificity, low sensitivity and weak anti-interference signal [130]. 2D materials have been proven to have a variety of properties that are much beneficial for biochemical sensing [131–134], for instance, a novel 2D g-C_3N_4-based aptamer PEC sensor has been made for Microcystin-LR (MC-LR) detection [135], surface modified MoS_2 nanocomposites used as photoelectrically active materials [136], 2D graphene-like TiO_2 nanosheets and carbon dots assembled as PEC sensor for pentachlorophenol detection [137]. Although 2D materials show excellent performance in PEC, the application of 2D materials- based membrane in PEC have been seldom reported. COFs have been widely used in PEC, while the poor solubility of COFs seriously limits the fabrication processibility. COF free-standing thin membrane (from 4 nm to 150 nm) named $COF_{TTA\text{-}DHTA}$ with high Young's modulus (25.9 ± 0.6 GPa) has been successfully prepared by a new type of interfacial polymerization method [138]. $COF_{TTA\text{-}DHTA}$ showed the responsiveness performance of PEC sensors for Ru^{3+}. Under the on-off Xe lamp illumination, $COF_{TTA\text{-}DHTA}$ generated about 1.2 μA/cm^2 photocurrent while the blank ITO did not show a significant response (Figs. 10a and b). Similarly, Zhang's group reported 2D COF film-based PEC electrodes (D-TA COF film/ITO), the photocurrent of the D-TA COF film grown on the ITO surface *in situ* was about 333 times higher than that of the randomly oriented D-TA COF powder drop-coated on ITO due to the crystalline oriented structure [139]. Although 2D materials show unique properties in PEC sensors, there are still some problems to overcome such as fabrication methods and applications of 2D materials based membrane materials.

2D materials have received much attention due to their outstanding mechanical properties, such as high Young's modulus and strength. Therefore, 2D materials are more likely to show potentials in pressure sensors [14]. In 2013, a stretchable self-healing film with self-activated pressure sensitivity has been reported, GO was used as the high strength performance provider [140], 2D materials are gradually emerging in biological sensors.

In order to overcome the limitations of polymer active materials, such as slow response speed and violent operation methods, Zhu's group used functional graphene to build a self-folding paper and explored its potentials in sensing, artificial muscles and robots, the paper was composed of rGO and the modified GO with polydopamine (PDA) [141]. The cross-shaped GO-PDA/rGO paper could fold itself under NIR light in about 200 ms. The programmable driving behavior of the GO-PDA/rGO paper demonstrated the advantages of 2D materials in bio-device applications.

In terms of strong and flexible characteristics, 2D materials also show great prospects for wearable and flexible electronic applications. A kind of composite membrane consisted of 2D Ti_3C_2 and natural microcapsule (NMC) applied as flexible pressure sensors have been reported by Shen's group [142]. When attached to the finger with tape, the Ti_3C_2/NMC flexible pressure sensor could monitor the continuous bending angle of the finger, the current would change with the change of the bending angle, so as to realize the function of real-time observation of the flexibility of the joint. Besides the intrinsic characteristics of 2D materials, it is of great significance to construct and design the microstructures and chemical modifications of 2D materials in order to extend further applications in biomimetic devices and sensors.

4.5. Catalytic membrane

2D materials exhibit various unique performances such as photocatalytic activity and have shown advantages over traditional materials in many fields. For example, g-C_3N_4 had emerged as a promising material for high-performance membranes with filtration and catalytic capabilities. As a new non-metallic photocatalytic material, g-C_3N_4 exhibits a wider absorption spectrum than the traditional TiO_2 photocatalyst and can play a photocatalytic role under ordinary visible light without ultraviolet light. In addition, g-C_3N_4 is more effective in activating molecular oxygen and generating superoxide free radicals for the photocatalytic transformation of organic functional groups and degradation of organic pollutants [143]. Assemble g-C_3N_4 sheets into membranes or lamellar structures can effectively achieve the combination of catalytic activity and separation ability, which has attracted more and more attention. Zhou *et al.* reported the membrane photoreactor (MPR) composed of g-C_3N_4 nanosheets assembled by vacuum filtration [144]. Using this reactor, organic dyes in water could be converted into non-hazardous compounds. As shown in Fig. 11a, the conversion rate for Sudan orange G (SG) of the bulk and membrane in the darkness was only 5.4%. As a comparison, the conversion rates for three kinds of dye reached more than 95% under light irradiation, proving the conversion efficiency has resulted from the catalytic degradation ability of g-C_3N_4. Additionally, the MPRs obtained by different preparation methods also had different conversion rates for the three dyes, which was due to the characteristic structure of the g-C_3N_4 membrane that allowed water to flow between layers and maximized the number of catalytic active centers at the solution-catalyst interface. Therefore, the degradation efficiency of the g-C_3N_4 membrane was enhanced with the solution permeating through the membrane, which was attributed to the increase in the number of available active sites (Fig. 11b).

In addition, the carbon nitride membranes can be modified by catalytic functional groups in order to enhance the catalytic performance. Lan's team intercalated the Fe-containing polyoxometalates (Fe-POMs) into the carbon nitride membranes, and obtained the U-g-C_3N_4/Fe-POMs composite membranes through the self-assembly method. The addition of Fe-POMs not only enhanced the stability of the self-assembled membranes, but also provided more active catalytic sites to effectively isolate the pollutant molecules [145]. As shown in Fig. 11c, the membrane absorbed light energy from the irradiation and excited to generate electrons (e^-) and holes (H^+) with the energy higher than its threshold. The photogenerated electrons and holes migrated to the surface of the membrane. The electrons were captured by dissolved oxygens to form super

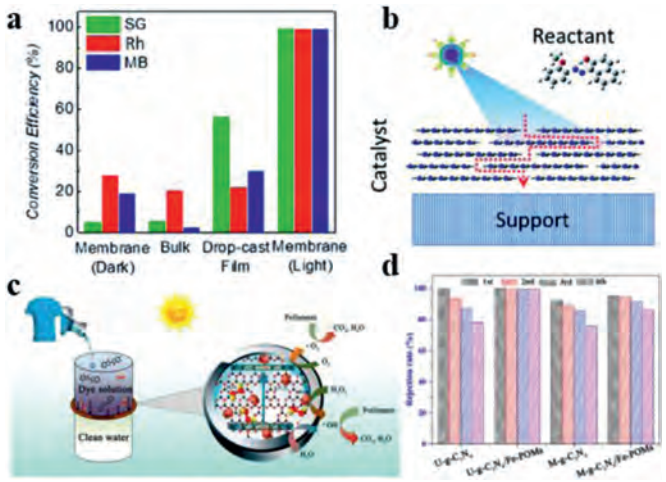

Fig. 11. (a) Conversion efficiency measured after 2 h using three different types of g-C_3N_4 (bulk g-C_3N_4, drop casted g-C_3N_4 membrane and g-C_3N_4 laminates obtained by filtration). A control experiment in the dark was also performed for the g-C_3N_4 laminates to evaluate the adsorption ability of the membrane. (b) Schematic of 2D nanosheets-based reactor for photodegradation. (a, b) Reprinted with permission [144]. Copyright 2017, American Chemical Society. (c) Schematic mechanism of water purification using U-g-C_3N_4/Fe-POMs photo-Fenton-like membranes. (d) Rejection rates and water flux of U-g-C_3N_4/Fe-POMs membranes for cyclic separation experiments. (c, d) Reprinted with permission [145]. Copyright 2019, American Chemical Society.

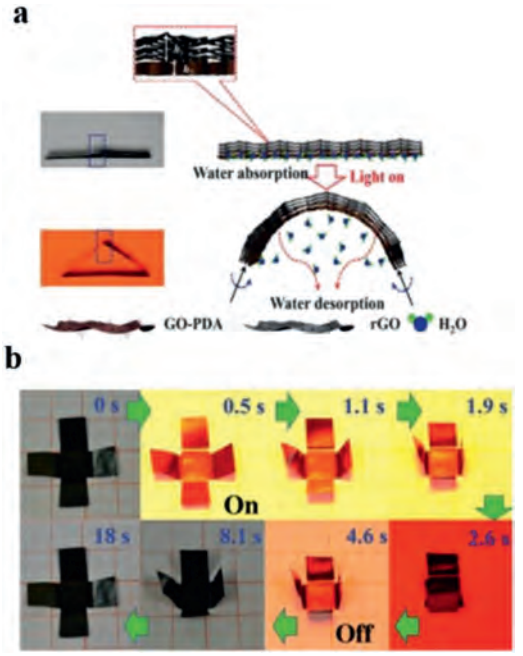

Fig. 12. (a) Schematic representations of the structures and mechanisms of the graphene paper. If there is no NIR light irradiation, the GO-PDA/rGO region flattens. A flat, freestanding GO-PDA/rGO region starts to bend immediately upon exposure to NIR light irradiation. This bending/unbending mechanism is completely reversible over many cycles. (b) Time profiles of self-folding movements of a cross-shaped piece of paper with and without NIR light irradiation. The sample was placed on the platform and illuminated with NIR light (100 mW/cm^2) normal to its surface (light is incident from above). Reprinted with permission [141]. Copyright 2015, Science.

oxygen free radicals (O^{2-}). While, the cavities were absorbed on the surface, resulting in the oxidation of water and hydroxide ions into hydroxyl radicals. These radicals had a strong oxidizing ability to degrade contaminants/bacteria on the surface into CO_2 and H_2O, achieving the effect of purification. The U-g-C_3N_4/Fe-POMS membranes exhibited nearly 100% rejections for the sewage during 4 cycles, demonstrating excellent stability and durability in wastewater treatment (Fig. 11d). Using the same principle, Fan's team introduced quantity tunable mesoporous g-C_3N_4 to extract U(VI) from water [146]. After the test under seawater conditions, the U(VI) in seawater was extracted within 20 min after the illumination started, and the concentration of U(VI) changed sharply, presenting the fine responsive characteristics of the membrane.

2D materials-based catalytic membranes show potentials for water purification and wastewater treatment. It is of great significance to design and optimize the interactions between 2D materials and other functional groups/molecules in order to obtain the enhanced catalytic performances and durability for practical applications.

4.6. Actuator

The varieties of applications in artificial muscles [147], controlled displays [148], robots [149] and so on have attracted a great deal of attention on actuators. Actuators can perform the mechanical deformation under external stimuli such as light intensity [150–152], humidity [152–154] and temperature [154,155]. There are different kinds of mechanical deformations of actuators including expansion-contraction [156,157], rotation [158,159], bending [160,161] and so on. Polymers with large-deformation ability are the most widely used materials for smart actuators. For example, PNIPAM or its ramification is one of the most important expansion-contraction actuators. Unfortunately, polymer materials exhibit poor mechanical properties, slow response speed and violent operation methods, which seriously hindering their practical applications. As a comparison, 2D materials with excellent mechanical strength and abundant functional groups are good candidates for smart actuators.

Zhu's group reported functional graphene to build a self-folding film and explored its potentials in sensing, artificial muscles and robots. The composite film was composed of rGO and PDA modified GO (Fig. 12a) [141]. The cross-shaped GO-PDA/rGO paper could fold itself under NIR light in about 200 ms (Fig. 12b). The programmable driving behavior of the GO-PDA/rGO paper demonstrated the advantages of 2D materials in actuator applications.

The fully 2D material-based actuator without the addition of other polymers is not limited by the defects of these materials. In addition, there are many advantages including easy fabrication, low cost and good flexibility. In 2010, Qu's group first reported the monolithic rGO actuator with asymmetrically modified surfaces [162]. One side of the rGO membrane was treated by oxygen plasma to become hydrophilic with a contact angle of 15° The other was applied the hydrophobic treatment by *n*-hexane plasma with the contact angle of 90° Thus, the rGO film exhibited asymmetrical electrochemical activities and deformation under the applied voltage with a maximum bending rate of 0.6 cm^{-1}. Based on the density gradient and upward convection flow during the solvent evaporation process of drop-casting, Zheng *et al.* fabricated the hierarchically structured GO film with cyclic temperature responsiveness [163,164]. The reliable curvature actuation resulted from the unique gradient structure of the GO film. Yang *et al.* reported the first homogeneous GO film actuator driven by a water-related trigger [165]. The actuation of the GO film was achieved by the *in-situ* formation of the bilayer structure upon triggering the GO film under the humidity gradient. This homogeneous GO actuator exhibited high sensitivity to the stimuli of humidity gradients and displayer continuous motion.

In order to enhance the deformation ability and sensitivity, 2D materials-based actuators composed of two different materials were reported thereby. Sun *et al.* fabricated the bilayer GO/rGO film by vacuum filtrating GO and rGO dispersion respectively [166].

Under the voltage of 24 V, the temperature of the GO/rGO bilayer film increased, resulting in the bending of the bilayer film to the GO side with the curvature of 0.5 cm^{-1}. Shi's team used submicron GO (SGO) with a small lateral size and reported the enhanced sensitivity of the SGO/RGO bilayer actuator [38]. This actuator showed potentials in soft robots with load-lifting and walking ability actuated by humidity. To fabricate the integrated structure of the GO-based actuator, varieties of strategies including partial reduction of the GO films by Cu foil [167], focused sunlight [168], UV light [169] and laser [64,170] have been reported to obtain asymmetric and integrated GO/rGO papers. These integrated GO/rGO actuators exhibited stable responsiveness to different external stimuli.

With the comprehensive development of artificial intelligence, the smart actuator has also become the research hotspot. There are two research directions for the 2D materials based smart actuator: One direction is the mini-actuator with excellent controllability to achieve potentials in human microstructure in replacement of traditional mechanical motors; The other is a large-area actuator with brilliant sensitivity and deformability to obtain large-scale practical applications and meet the demands of lifting kilos or even tons of industrialized weight. It is still a challenge to enhance the sensitivity and deformability of the 2D materials-based smart actuators synchronously up to now.

5. Conclusion and outlook

Significant progress has been made on 2D materials-based smart responsive devices to control mass transport and molecular conversions. Taking advantage of the ultrahigh molecular transport, high permeability, fast and significant response to the external stimuli and long-term stability 2D materials has stimulated much enthusiasm for ultrathin and highly selective smart membranes. With carefully designed responsive groups, 2DSMs can efficiently tune the mass transport and molecular conversion by variable external stimuli, including pH, magnetic field, electric field, light and temperature. Endowed by the efficient controllability, 2DSMs have shown great potential in the applications of membrane separation, pressure sensors, blue energy harvesting, photoelectrochemical sensors and biomimetic devices, opening a new avenue towards the industrialization of 2DSMs in the chemical engineering, bioengineering and environmental protection.

However, a few challenges remain to be solved before the next step towards the practical applications of 2DSMs. Firstly, the responsive mechanism in 2DSMs needs to be further explored. Compared to polymetric membranes, 2DSMs with highly order nanocapillary have exhibited phenomenal properties, *e.g.*, ultrafast mass transport and efficient molecular conversion. However, present understandings on the controlling effects are still based on previous theories in polymer physics, which may not suitable to understand the extraordinary phenomenon in 2DSMs. By introducing state-of-art tools, more details on the mass transport and molecular conversion would help to expand the understanding of the tunable nanofluidics in 2D nanocapillary and inspire the new design of efficient 2DSMs. Secondly, compared to the natural smart membranes, the sensitivity, reversibility, and specificity of the responsive 2DSMs need to be further improved. Most of the membrane proteins are only responsive to one or few characteristic signal molecules or ions, while other environmental changes are not able to control the mass transport or molecular conversions. However, the 2DSMs can be tuned by variable factors, *e.g.*, pH, temperature, light, chemical potential. Consequently, the different factors in practical applications may bring contradictory effects and thus reduce the responsivity. Therefore, the recognition of 2DSMs under the interference from environmental variations should be examined. In addition, the trade-off relationship between mechanical strength and the permeability of 2DSMs still remains further exploration to meet the demands in practical and industrialized applications.

Declaration of competing interest

The authors declare no conflict of interests.

Acknowledgments

This work was supported by the National Science Foundation of China (No. 21972105, 2020), Open Project of The National Laboratory of Solid State Microstructures, Nanjing University (No. M33028, 2020) and 1000 Talent Program for Young Scientists; Key Laboratory of Special Functional Materials and Structural Design of Ministry of Education (Class B), Lanzhou University (No. lzujbky-2021-kb06).

References

[1] P. Agre, S. Sasaki, M.J. Chrispeels, Am. J. Physiol. 265 (1993) F461.
[2] P.D. Boyer, Paul D. Boyer, Les Prix Nobel 1977 (1998) 177–185.
[3] Z. Liu, W. Wang, R. Xie, X.J. Ju, L.Y. Chu, Chem. Soc. Rev. 45 (2016) 460–475.
[4] L. Wang, M.S.H. Boutilier, P.R. Kidambi, et al., Nat. Nanotechnol. 12 (2017) 509–522.
[5] H.B. Park, J. Kamcev, L.M. Robeson, M. Elimelech, B.D. Freeman, Science 356 (2017) 6343.
[6] M. Galizia, W.S. Chi, Z.P. Smith, et al., Macromolecules 50 (2017) 7809–7843.
[7] A.K. Geim, K.S. Novoselov, Nat. Mater. 6 (2007) 183–191.
[8] M. Fathizadeh, W.W.L. Xu, F.L. Zhou, Y. Yoon, M. Yu, Adv. Mater. 4 (2017) 1600918.
[9] S. Gadipelli, Z.X. Guo, Prog. Mater. Sci. 69 (2015) 1–60.
[10] J. Shen, G.P. Liu, Y. Han, W.Q. Jin, Nat. Rev. Mater. 6 (2021) 294–312.
[11] X.W. Yu, H.H. Cheng, M. Zhang, et al., Nat. Rev. Mater. 2 (2017) 17020.
[12] R.R. Nair, H.A. Wu, P.N. Jayaram, I.V. Grigorieva, A.K. Geim, Science 335 (2012) 442–444.
[13] A. Keerthi, A.K. Geim, A. Janardanan, et al., Nature 558 (2018) 420–424.
[14] F. Perreault, A. Fonseca de Faria, M. Elimelech, Chem. Soc. Rev. 44 (2015) 5861–5896.
[15] S. Wang, L. Yang, G. He, et al., Chem. Soc. Rev. 49 (2020) 1071–1089.
[16] Z. Zhu, D. Wang, Y. Tian, L. Jiang, J. Am. Chem. Soc. 22 (2019) 8658–8669.
[17] R.K. Joshi, P. Carbone, F.C. Wang, et al., Science 343 (2014) 752–754.
[18] L. Dai, F. Xu, K. Huang, et al., Angew. Chem. Int. Ed. 60 (2021) 19933–19941.
[19] A.C. Ferrari, F. Bonaccorso, V. Fal'ko, et al., Nanoscale 7 (2015) 4598–4810.
[20] M. W.Barsoum, Prog. Chem. 28 (2000) 201–281.
[21] Z.K. Li, Y. Wei, X. Gao, et al., Angew. Chem. Int. Ed. 59 (2020) 9751–9756.
[22] J. Zhu, L. Wang, J. Wang, et al., ACS Nano 14 (2020) 15306–15316.
[23] J. Wang, Z. Zhang, J. Zhu, et al., Nat. Commun. 11 (2020) 5917.
[24] L. Ding, L. Li, Y. Liu, et al., Nat. Sustain. 3 (2020) 296–302.
[25] Q. Weng, X. Wang, X. Wang, Y. Bando, D. Golberg, Chem. Soc. Rev. 45 (2016) 3989–4012.
[26] Q.H. Wang, K. Kalantar-Zadeh, A. Kis, J.N. Coleman, M.S. Strano, Nat. Nanotechnol. 7 (2012) 699–712.
[27] X. Zhang, Z. Lai, C. Tan, H. Zhang, Angew. Chem. Int. Ed. 55 (2016) 8816–8838.
[28] Q. Wang, D. O'Hare, Chem. Rev. 112 (2012) 4124–4155.
[29] S.P. Koenig, R.A. Doganov, H. Schmidt, A.H.C. Neto, B. Ozyilmaz, Appl. Phys. Lett. 104 (2014) 103106.
[30] H. Wang, Z. Zeng, P. Xu, et al., Chem. Soc. Rev. 48 (2019) 488–516.
[31] S. Yuan, X. Li, J. Zhu, et al., Chem. Soc. Rev. 48 (2019) 2665–2681.
[32] Y. Guo, X.S. Peng, Sci. China Mater. 62 (2019) 25–42.
[33] Y. Zheng, J. Liu, J. Liang, M. Jaroniec, S.Z. Qiao, Energy Environ. Sci. 5 (2012) 6717–6731.
[34] X. Wang, C. Chi, K. Zhang, et al., Nat. Commun. 8 (2017) 14460.
[35] A. Fang, K. Kroenlein, D. Riccardi, A. Smolyanitsky, Nat. Mater. 18 (2019) 76–81.
[36] A. Fang, K. Kroenlein, A. Smolyanitsky, J. Phys. Chem. C 123 (2019) 3588–3593.
[37] A. Achari, S. Sahana, M. Eswaramoorthy, Energy Environ. Sci. 9 (2016) 1224–1228.
[38] C. Tan, X. Cao, X.J. Wu, et al., Chem. Rev. 117 (2017) 6225–6331.
[39] J.P. Thiruraman, S.A. Dar, P.M. Das, et al., Sci. Adv. 6 (2020) eabc7927.
[40] J. Feng, K. Liu, M. Graf, et al., Nano Lett. 15 (2015) 3431–3438.
[41] J.M. Alaboson, Q.H. Wang, J.A. Kellar, et al., Adv. Mater. 23 (2011) 2181–2184.
[42] K. Chen, X. Wan, J. Wen, et al., ACS Nano 9 (2015) 9868–9876.
[43] D. Dumcenco, D. Ovchinnikov, K. Marinov, et al., ACS Nano 9 (2015) 4611–4620.
[44] P. Gallagher, M. Lee, F. Amet, et al., Nat. Commun. 7 (2016) 13612.
[45] P. Hapala, G. Kichin, C. Wagner, et al., Phys. Rev. B 90 (2014) 085421.
[46] G.J. Hedley, A.J. Ward, A. Alekseev, et al., Nat. Commun. 4 (2013) 3017.
[47] J.A. Kellar, J.M. Alaboson, Q.H. Wang, M.C. Hersam, Appl. Phys. Lett. 96 (2010) 143103.
[48] S.Y. Leblebici, L. Leppert, Y. Li, et al., Nat. Energy 1 (2016) 16039.

[49] C. Lei, A. Das, M. Elliott, J.E. Macdonald, Nanotechnology 15 (2004) 627.
[50] M.Y. Li, Y. Shi, C.C. Cheng, et al., Science 349 (2015) 524–528.
[51] Y. Li, C.Y. Xu, L. Zhen, Appl. Phys. Lett. 102 (2013) 143110.
[52] X. Liu, I. Balla, H. Bergeron, et al., ACS Nano 10 (2016) 1067–1075.
[53] X. Liu, M.C. Hersam, Adv. Mater. 30 (2018) 1801586.
[54] G.D. Nguyen, H.Z. Tsai, A.A. Omrani, et al., Nat. Nanotechnol. 12 (2017) 1077–1082.
[55] V.K. Sangwan, D. Jariwala, I.S. Kim, et al., Nat. Nanotechnol. 10 (2015) 403–406.
[56] I. Sharma, B. Mehta, Appl. Phys. Lett. 110 (2017) 061602.
[57] M. Tosun, D. Fu, S.B. Desai, et al., Sci. Rep. 5 (2015) 1–8.
[58] D. Wong, J. Velasco, L. Ju, et al., Nat. Nanotechnol. 10 (2015) 949–953.
[59] Z. Zhao, X. Chen, H. Wu, X. Wu, G. Cao, Adv. Funct. Mater. 26 (2016) 3048–3058.
[60] D. Cohen-Tanugi, L.C. Lin, J.C. Grossman, Nano Lett. 16 (2016) 1027–1033.
[61] K. Nieszporek, M. Drach, Phys. Chem. Chem. Phys. 17 (2015) 1018–1024.
[62] J. Yang, X.J. Loh, B.H. Tan, Z. Li, Macromol. Rapid Commun. 40 (2019) 1800013.
[63] M.A. Abbas, S. Mushtaq, W.A. Cheema, et al., Adv. Polym. Technol. 2020 (2020) 8281058.
[64] Z. Cai, J. Shi, W. Li, et al., ACS Appl. Mater. Interfaces 11 (2019) 28228–28235.
[65] X. Zhu, Y. Zhou, J. Hao, et al., ACS Nano 11 (2017) 10816–10824.
[66] L. Zhang, A. Ghaffar, X. Zhu, B. Chen, Environ. Sci. Technol. 53 (2019) 10398–10407.
[67] D.V. Andreeva, M. Trushin, A. Nikitina, et al., Nat. Nanotechnol. 16 (2021) 174–180.
[68] L. Chen, G. Shi, J. Shen, et al., Nature 550 (2017) 415–418.
[69] Q. Yang, H.H. Himstedt, M. Ulbricht, X. Qian, S.R. Wickramasinghe, J. Membr. Sci. 430 (2013) 70–78.
[70] Y. Wang, Y. Huang, Y. Song, et al., Nano Lett. 9 (2009) 220–224.
[71] F. Lin, G. Yang, C. Niu, et al., Adv. Funct. Mater. 28 (2018) 1805255.
[72] F. Lin, Z. Zhu, X. Zhou, et al., Adv. Mater. 29 (2017) 1604453.
[73] P. Sun, F. Zheng, K. Wang, et al., Sci. Rep. 4 (2014) 6798.
[74] M. Rastgar, A. Shakeri, A. Bozorg, H. Salehi, V. Saadattalab, Appl. Surf. Sci. 441 (2018) 923–935.
[75] M. Gibertini, M. Koperski, A.F. Morpurgo, K.S. Novoselov, Nat. Nanotechnol. 14 (2019) 408–419.
[76] W. Ying, K. Zhou, Q. Hou, et al., J. Mater. Chem. A 7 (2019) 15062–15067.
[77] X. Zhang, M. Jia, L. Wang, et al., Phys. Status. Solidi. Rapid Res. Lett. 13 (2019) 1900129.
[78] J. Yang, W. Zhu, X. Zhang, F. Chen, L. Jiang, New J. Chem. 43 (2019) 7190–7193.
[79] K.G. Zhou, K.S. Vasu, C.T. Cherian, et al., Nature 559 (2018) 236–240.
[80] J. Xiao, H. Zhan, X. Wang, et al., Nat. Nanotechnol. 15 (2020) 683–689.
[81] Y. Wang, H. Zhang, Y. Kang, et al., ACS Nano 13 (2019) 11793–11799.
[82] X. Zhang, Q. Wen, L. Wang, et al., ACS Nano 13 (2019) 4238–4245.
[83] Q. Wen, P. Jia, L. Cao, et al., Adv. Mater. 32 (2020) 1903954.
[84] Y. Liu, Y. Su, J. Guan, et al., Adv. Funct. Mater. 28 (2018) 1706545.
[85] Y. Zhang, F. Li, X. Kong, et al., Adv. Funct. Mater. 30 (2020) 1907549.
[86] J. Lao, R. Lv, J. Gao, et al., ACS Nano 12 (2018) 12464–12471.
[87] L. Wang, Q. Wen, P. Jia, et al., Adv. Mater. 31 (2019) 1903029.
[88] Y. Zhang, G. Zhao, H. Zhu, L. Jiang, Chem. Commun. 56 (2020) 9819–9822.
[89] D. Quan, D. Ji, Q. Wen, et al., Adv. Funct. Mater. 30 (2020) 2001549.
[90] P. Zhang, F. Liu, Q. Liao, et al., Angew. Chem. Int. Ed. 57 (2018) 16343–16347.
[91] S. Hong, F. Ming, Y. Shi, et al., ACS Nano 13 (2019) 8917–8925.
[92] P. Yang, H. Wu, N.A. Khan, et al., J. Membr. Sci. 606 (2020) 118136.
[93] H. Liu, J. Zhu, L. Hao, et al., J. Membr. Sci. 587 (2019) 117163.
[94] J. Liu, L.J. Yu, G. Yue, et al., Adv. Funct. Mater. 29 (2019) 1808501.
[95] J. Liu, N. Wang, L.J. Yu, et al., Nat. Commun. 8 (2017) 2011.
[96] A. Halperin, M. Kroger, F.M. Winnik, Angew. Chem. Int. Ed. 54 (2015) 15342–15367.
[97] J. Dong, J. Weng, L. Dai, Carbon 52 (2013) 326–336.
[98] W. Jia, B. Wu, S. Sun, P. Wu, Nano Res. 13 (2020) 2973–2978.
[99] F. Gallucci, E. Fernandez, P. Corengia, M.V. Annaland, Chem. Eng. Sci. 92 (2013) 40–66.
[100] A. Huang, H. Bux, F. Steinbach, J. Caro, Angew. Chem. Int. Ed. 49 (2010) 4958–4961.
[101] C. Rubio, B. Zornoza, P. Gorgojo, C. Tellez, J. Coronas, Curr. Org. Chem. 18 (2014) 2351–2363.
[102] B. Li, G. He, X. Jiang, Y. Dai, X. Ruan, Front. Chem. Sci. Eng. 10 (2016) 255–264.
[103] K. Ramasubramanian, Y. Zhao, W.S.W. Ho, AIChE J. 59 (2013) 1033–1045.
[104] T.C. Merkel, H. Lin, X. Wei, R. Baker, J. Membr. Sci. 359 (2010) 126–139.
[105] M. Rezakazemi, A.E. Amooghin, M.M. Montazer-Rahmati, A.F. Ismail, T. Matsuura, Prog. Polym. Sci. 39 (2014) 817–861.
[106] J.A. Mason, T.M. McDonald, T.H. Bae, et al., J. Am. Chem. Soc. 137 (2015) 4787–4803.
[107] H.W. Kim, H.W. Yoon, S.M. Yoon, et al., Science 342 (2013) 91–95.
[108] J. Shen, G. Liu, K. Huang, et al., ACS Nano 10 (2016) 3398–3409.
[109] F. Zhou, H.N. Tien, W.L. Xu, et al., Nat. Commun. 8 (2017) 14675.
[110] L. Dong, M. Chen, J. Li, et al., J. Membr. Sci. 520 (2016) 801–811.
[111] D. Kim, M.Y. Jeon, B.L. Stottrup, M. Tsapatsis, Angew. Chem. Int. Ed. 57 (2018) 480–485.
[112] M.Y. Jeon, D. Kim, P. Kumar, et al., Nature 543 (2017) 690–694.
[113] K.V. Agrawal, B. Topuz, Z. Jiang, et al., AIChE J. 59 (2013) 3458–3467.
[114] L. Ding, Y. Wei, L. Li, et al., Nat. Commun. 9 (2018) 155.
[115] J. Liu, H.B. Zhang, R. Sun, et al., Adv. Mater. 29 (2017) 1702367.
[116] J. Shen, G. Liu, Y. Ji, et al., Adv. Funct. Mater. 28 (2018) 1801511.
[117] H. Fan, A. Mundstock, A. Feldhoff, et al., J. Am. Chem. Soc. 140 (2018) 10094–10098.
[118] V.A. Kuehl, J. Yin, P.H.H. Duong, et al., J. Am. Chem. Soc. 140 (2018) 18200–18207.
[119] B.P. Biswal, H.D. Chaudhari, R. Banerjee, U.K. Kharul, Chemistry (Easton) 22 (2016) 4695–4699.
[120] C.S. Diercks, O.M. Yaghi, Science 355 (2017) 966–969.
[121] Y. Peng, Y. Li, Y. Ban, et al., Science 346 (2014) 1356–1359.
[122] Y. Peng, Y. Li, Y. Ban, W. Yang, Angew. Chem. Int. Ed. 56 (2017) 9757–9761.
[123] S. Ma, D. Sun, X.S. Wang, H.C. Zhou, Angew. Chem. Int. Ed. 46 (2007) 2458–2462.
[124] W. Li, W. Wu, Z. Li, ACS Nano 12 (2018) 9309–9317.
[125] L. Ries, E. Petit, T. Michel, et al., Nat. Mater. 18 (2019) 1112–1117.
[126] L. Wang, Y. Feng, Y. Zhou, et al., Chem. Sci. 8 (2017) 4381–4386.
[127] C. Cheng, G. Jiang, G.P. Simon, J.Z. Liu, D. Li, Nat. Nanotechnol. 13 (2018) 685–690.
[128] J. Feng, M. Graf, K. Liu, et al., Nature 536 (2016) 197–200.
[129] Y. Liang, F. Zhao, Z.H. Cheng, et al., Energy Environ. Sci. 11 (2018) 1730–1735.
[130] J.P. Tian, H.M. Zhao, X. Quan, et al., Sens. Actuator. B: Chem. 196 (2014) 532–538.
[131] D. Tyagi, H. Wang, W. Huang, et al., Nanoscale 12 (2020) 3535–3559.
[132] P. Jiang, Y.F. Li, T. Ju, et al., Chem. Res. Chin. Univ. 36 (2020) 307–312.
[133] A. Bolotsky, D. Butler, C. Dong, et al., ACS Nano 13 (2019) 9781–9810.
[134] N. Rohaizad, C.C. Mayorga-Martinez, Z. Sofer, M. Pumera, ACS Appl. Mater. Interfaces 9 (2017) 40697–40706.
[135] Y. Li, Y. Bu, F. Jiang, X. Dai, J.P. Ao, Biosens 150 (2020) 111903.
[136] X. Wang, H. Deng, C. Wang, et al., Analyst 145 (2020) 1302–1309.
[137] X.C. Fu, J. Zhang, W. Gan, L. Bao, J. Electrochem. Sci. 167 (2020) 046513.
[138] Q. Hao, C. Zhao, B. Sun, et al., J. Am. Chem. Soc. 140 (2018) 12152–12158.
[139] T. Liu, L. Cui, H. Zhao, X. Zhang, ACS Appl. Mater. Interfaces 12 (2020) 47090–47098.
[140] C. Hou, T. Huang, H. Wang, et al., Sci. Rep. 3 (2013) 3138.
[141] J. Mu, C. Hou, H. Wang, et al., Sci. Adv. 1 (2015) e1500533.
[142] K. Wang, Z. Lou, L. Wang, et al., ACS Nano 13 (2019) 9139–9147.
[143] A.L. Linsebigler, G. Lu, J.T. Yates Jr, Chem. Rev. 95 (1995) 735–758.
[144] K.G. Zhou, D. McManus, E. Prestat, et al., J. Mater. Chem. A 4 (2016) 11666–11671.
[145] H. Lan, F. Wang, M. Lan, et al., Environ. Sci. Technol. 53 (2019) 6981–6988.
[146] J.J. Wang, Y. Wang, W. Wang, et al., Chem. Eng. J. 383 (2020) 123193.
[147] J. Mu, M. Jung de Andrade, S. Fang, et al., Science 365 (2019) 150–155.
[148] L. Ji, Y. Yu, Q. Deng, S. Shen, Nanoscale 12 (2020) 15643–15651.
[149] Y.Y. Yang, Y.T. Liu, Y.J. Shen, Adv. Funct. Mater. 30 (2020) 1910172.
[150] J. Lee, S. Oh, J. Pyo, J.M. Kim, J.H. Je, Nanoscale 7 (2015) 6457–6461.
[151] L. Hines, K. Petersen, M. Sitti, Adv. Mater. 28 (2016) 3690–3696.
[152] L. Chen, M. Weng, P. Zhou, et al., Nanoscale 9 (2017) 9825–9833.
[153] A.Le Duigou, M. Castro, Ind. Crops Prod. 71 (2015) 290–298.
[154] G. Xu, M. Zhang, Q. Zhou, et al., Nanoscale 9 (2017) 17465–17470.
[155] Y. Wang, K. Li, X.G. Li, et al., Carbon 152 (2019) 873–881.
[156] S. Jiang, F. Liu, A. Lerch, L. Ionov, S. Agarwal, Adv. Mater. 27 (2015) 4865–4870.
[157] B. Zuo, M. Wang, B.P. Lin, H. Yang, Chem. Mater. 30 (2018) 8079–8088.
[158] C.W. You, W.J. Qin, Z. Yan, et al., J. Mater. Chem. A 9 (2021) 10240–10250.
[159] Y. Song, S. Zhou, K. Jin, et al., Nanoscale 10 (2018) 4077–4084.
[160] X. Lu, H. Zhang, G. Fei, et al., Adv. Mater. 30 (2018) 1706597.
[161] Y. Yang, Z. Pei, Z. Li, Y. Wei, Y. Ji, J. Am. Chem. Soc. 138 (2016) 2118–2121.
[162] X. Xie, L. Qu, C. Zhou, et al., ACS Nano 4 (2010) 6050–6054.
[163] G.Z. Sun, Y.Z. Pan, Z.Y. Zhan, et al., J. Phys. Chem. C 115 (2011) 23741–23744.
[164] H. Cheng, F. Zhao, J. Xue, et al., ACS Nano 10 (2016) 9529–9535.
[165] Y. Ge, R. Cao, S. Ye, et al., Chem. Commun. 54 (2018) 3126–3129.
[166] H. Bi, K. Yin, X. Xie, et al., Nanoscale 5 (2013) 9123–9128.
[167] J. Mu, C. Hou, B. Zhu, et al., Sci. Rep. 5 (2015) 9503.
[168] H.B. Jiang, Y. Liu, J. Liu, et al., Front. Chem. 7 (2019) 464.
[169] D.D. Han, Y.L. Zhang, Y. Liu, et al., Adv. Funct. Mater. 25 (2015) 4548–4557.
[170] H. Cheng, J. Liu, Y. Zhao, et al., Angew. Chem. Int. Ed. 52 (2013) 10482–10486.